J Supercond Nov Magn (2017) 30:511–520
DOI 10.1007/s10948-016-3789-3

ORIGINAL PAPER

Electromagnetic Characterization of Co-Ti-Doped Ba-M Ferrite-Based Frequency-Tunable Microwave Absorber in 12.4–40 GHz

Sukhleen Bindra Narang[1] · Kunal Pubby[1]

Received: 28 June 2016 / Accepted: 31 August 2016 / Published online: 17 September 2016

Abstract The aim of the presented study is to characterize the electromagnetic and absorption properties of cobalt-titanium-substituted barium hexaferrites $BaCo_xTi_xFe_{12-2x}O_{19}$ ($x = 0.0$, 0.1, 0.3, 0.5, 0.7 and 0.9), synthesized by ceramic method, in 12.4–40 GHz frequency range. A vector network analyser was employed to investigate the complex permittivity and permeability. Doping of impurity ions has resulted in an increase in imaginary permittivity and permeability. Conductivity analysis has been done to understand its influence over the absorption properties. Reflection loss and transmission loss values have been determined experimentally on the ferrite pellets, and percentage absorption was calculated theoretically. Absorption analysis shows that all ferrites are observed to have 60 to 76 % average absorption in this frequency range. Samples $x = 0.3$ and $x = 0.7$ have achieved absorption peaks of 97.37 and 90.45 %, respectively, at 36.22 GHz frequency. A.C. conductivity, impedance and attenuation constant calculations have been made in order to support the observed trends in the studied properties. The entire absorption analysis of these ferrites suggests their application as a single-layer absorber in reducing the electromagnetic pollution and shaping of antenna patterns.

✉ Sukhleen Bindra Narang
sukhleen2@yahoo.com

[1] Department of Electronics Technology, Guru Nanak Dev University, Amritsar, Punjab, India

Keywords Barium hexaferrite · K band · Ka band · Electromagnetic properties · Absorption · Attenuation constant

1 Introduction

In the past few decades, microwave absorbing materials (MAMs) and radar absorbing materials (RAMs) have directed the scientific research towards themselves due to their expanding applications in different technical fields such as stealth defence system, microwave interference protection, microwave darkroom and industries [1, 2]. On the one hand, these are significant in controlling the levels of electromagnetic (EM) radiation emitted by electronic gadgets and antennas, while on the other hand, they are important in camouflaging the potential targets like aircrafts, ships and tanks from radar interception in wars [3, 4]. Wireless local area networks and antenna technology have also ushered in gigahertz frequency range. Due to the increasing demands of suppressing EM waves, many efforts have been made in a field of MAMs. For realization of MAMs, the incident EM wave must enter the material without front-end reflection and get attenuated rapidly to an acceptable low magnitude [5, 6]. To achieve the first condition, the material must have numerically equal values of complex permittivity and permeability and high losses in the frequency range. But, the ferrites have high values of permittivity and moderate values of permeability. The impedance matching is achieved by having a suitable sample thickness. High dielectric and magnetic losses are required for satisfaction of second condition. When the

wave illuminates the material, electric dipoles are formed which align themselves in the direction of applied field. This dipole alignment results in absorption of the energy while reflecting and transmitting the rest of the part [7, 8] as depicted in Fig. 1.

The reflected, transmitted and absorbed wave powers emerging from the material as a result of interaction are related to the incident wave power by the formula

$$P_{\text{incident}} = P_{\text{reflected}} + P_{\text{transmitted}} + P_{\text{absorbed}} \quad (1)$$

Depending on whether $P_{\text{reflected}}$ or P_{absorbed} is closer to P_{incident}, the material acts either as a reflector or absorber in a microwave band. For an effective microwave absorber, the absorbed power should be as close to the incident power as possible. For that, they must have large electric and magnetic losses in a specific frequency range. Ferrites, which produce spontaneous magnetization, maintain good dielectric properties and avoid skin effect at high frequency and thus have been regarded as a valuable electronic material absorber [9]. The losses in ferrites are generated by the changes in the alignment and rotation of magnetic spins [10]. The dependence of these losses on the frequency results in the scattering and/or absorption of the signal. In the last few years, variation in different properties of ferrites like cation distribution, resistivity, coercivity and permittivity has been reported by a substitution of base ion or ferric ion [11, 12]. But, most of the work has remained restricted up to X band or Ku band sometimes [13–15]. The higher bands (above 18 GHz) are very rarely studied. Impedance characterization and deep absorption analysis have remained unnoticed.

In the present investigation, we have analysed the modifications in electromagnetic properties of Co-Ti-substituted barium hexaferrites $BaCo_xTi_xFe_{12-2x}O_{19}$ ($x = 0.0$, 0.1, 0.3, 0.5, 0.7 and 0.9) in 12.4–40 GHz frequency range. Complex permittivity, A.C. conductivity and complex permeability of these ferrites are scrutinized in this frequency range to understand their contribution in the microwave absorption. Impedance characterization of ferrites has been done to seek out the origin of conduction mechanism. The variation of reflection, transmission and absorption of EM waves in the ferrite pellets in this frequency range is elaborated both qualitatively and quantitatively. This work has not been previously reported anywhere to the best of author's knowledge.

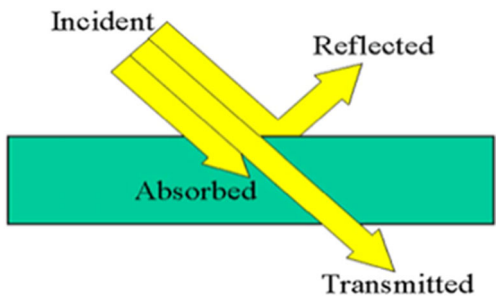

Fig. 1 Illustration of reflection, transmission and absorption mechanism

2 Experimental Procedure

The conventional solid-state reaction route was used to prepare the ferrite series under investigation. The complete structural and X band absorption characterization of these samples has been previously reported [16]. The presented work is an extension of that report where frequency of analysis has been increased up to 40 GHz. We have used a rectangular waveguide measurement technique as it produces more accurate results and less radiation loss than free-space measurement [17]. This method requires perfect fitting of the sample into the inner dimension of the waveguide at the frequency being measured. For Ku, K and Ka band measurements, pellets of ferrite material were shaped to fit exactly in rectangular waveguides WR-62 (15.79 mm ×7.89 mm), WR-42 (10.67 mm ×4.32 mm) and WR-28 (7.11 mm ×3.55 mm), respectively. Ferrites need a different degree of thickness to absorb microwaves in different frequency bands: 12.4–18 GHz (Ku band), 18–26.5 GHz (K band) and 26.5–40 GHz (Ka band). So, the samples of different thicknesses are prepared for the absorption analysis in the respective bands. Two-port calibration was done on both input and output ports to remove the errors due to mismatch. Scattering (S) parameters (S_{11}/S_{22} and S_{12}/S_{21}) were determined using an Agilent N5225A PNA series network analyser at room temperature. The Nicolson-Ross method [18] was utilized for determination of electromagnetic parameters like complex permittivity and complex permeability. Reflection loss (dB) and transmission loss (dB) were calculated from S parameters using the formula

$$\text{RL (dB)} = 20\log_{10}|S_{11}| \text{ and TL (dB)} = 20\log_{10}|S_{21}| \quad (2)$$

Absorption parameters were calculated from these two parameters by using (1).

3 Results and Discussion

Figure 2 illustrates the behaviour of real part of permittivity (ε') of the ferrites with respect to (w.r.t.) frequency in Ku, K and Ka bands. It can be clearly inferred from the plots that doping has resulted in lowering in the average value of ε' in these bands except for sample $x = 0.5$. Lower values of dielectric constant, obtained after the doping, are favourable from an impedance matching point of

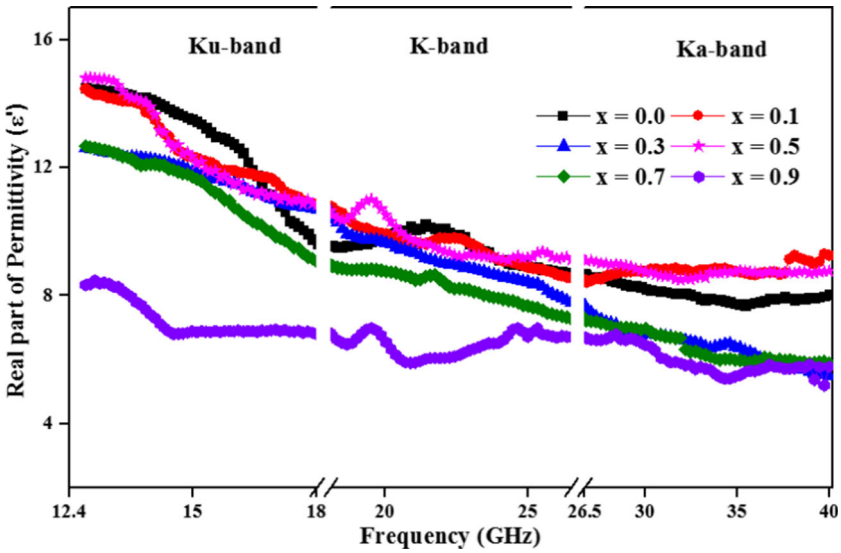

Fig. 2 Dependence of real permittivity (ε') of the ferrite material with frequency and composition

view, which further reduces the front-end reflection of EM wave [19]. It is seen that sample $x = 0.9$ has the lowest dielectric constant in all the three bands. All the samples show a fall in values of ε' in Ku band. Real permittivity, as depicted in Fig. 2, remains almost constant in K band and Ka band w.r.t. frequency. Dielectric characteristics of ferrite materials are governed by interfacial and electric dipole polarization [20]. The higher the polarization, the higher will be the real permittivity. As the frequency increases, these two parameters reduce and ultimately settle to very small insignificant values. Variation in Ku band is a consequence of the decrease in polarization, while the constant values achieved in the higher two bands indicate the settling to polarization to a particular level. Dong et al. have reported the real permittivity in the same range for doped barium hexaferrites [21].

The frequency dependence of imaginary part of permittivity (ε'') of the ferrites is displayed in Fig. 3. The dipolar polarization, interfacial polarization and the relaxation phenomena, associated with these, constitute the dielectric loss mechanisms in the ferrites. Also, multivalent iron ions Fe^{2+} and Fe^{3+} permits the hopping of excess electrons from one valence state to another. This results in electrical conduction, hence dielectric losses [22]. The matching of electron hopping frequency with the frequency of applied field results in the resonance peaks in permittivity spectra. The variation of dielectric loss w.r.t. frequency is almost similar to dielectric constant because governing factors are the same in both. Analysing the variation of ε'' w.r.t. doping level, it can be stated that the losses are enhanced with the combined substitution of cobalt and titanium. With the doping, the chances of hopping of electrons between tetrahedral

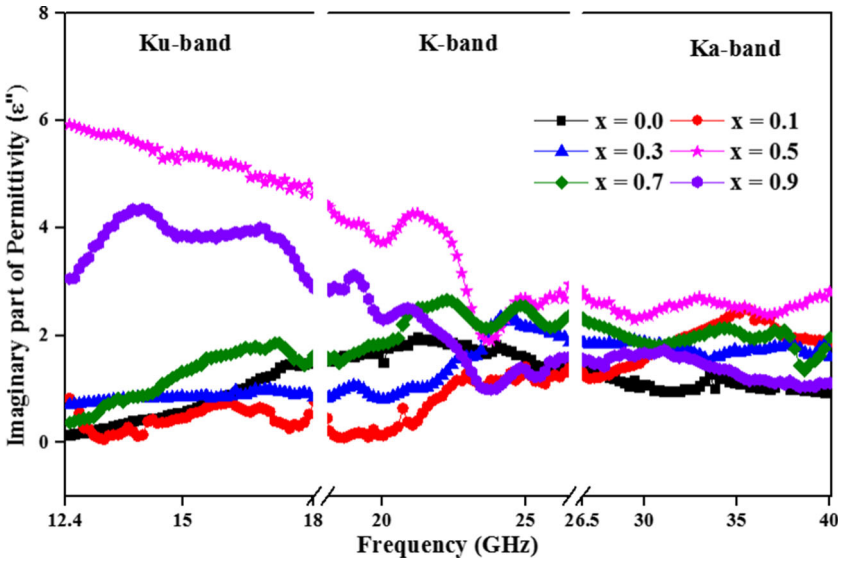

Fig. 3 Variation of imaginary permittivity (ε') of the ferrite material with frequency and composition

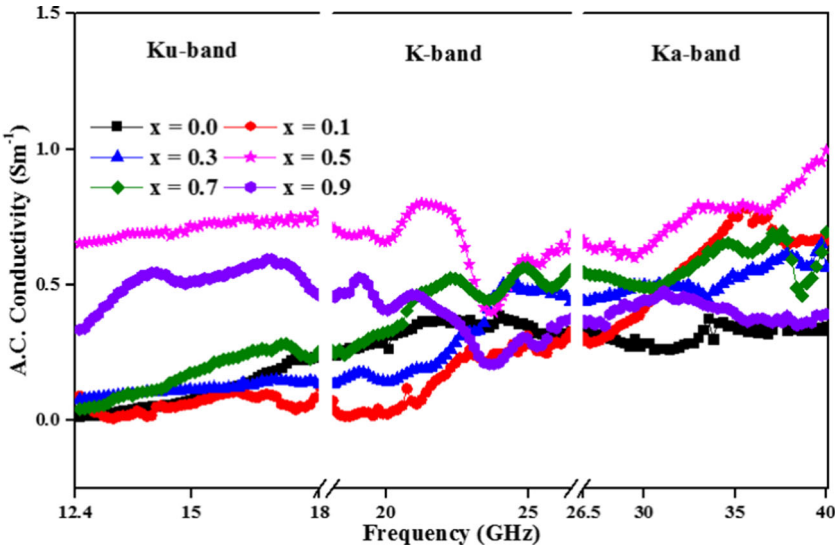

Fig. 4 Frequency dependence of A.C. conductivity (S, m^{-1}) of the prepared ferrites

and octahedral sites have increased, which has resulted in increased losses.

The dielectric properties are not only affected by the polarization and relaxation but also are remarkably affected by A.C. conductivity (σ). The Debye equation for permittivity clearly indicates this point [23]

$$\varepsilon = \varepsilon' - j\varepsilon'' = \varepsilon_\infty + \frac{\varepsilon_S - \varepsilon_\infty}{1 + j2\pi f\tau} - j\frac{\sigma}{2\pi f\varepsilon_0} \tag{3}$$

where f is the frequency, τ is the relaxation time, ε_0 is the vacuum permittivity and ε_S and ε_∞ are the stationary and optical relative permittivity, respectively. So, the variation of conductivity in 12.4–40 GHz frequency range for all the ferrite compositions is presented in Fig. 4 to explore its relation with absorption. Conductivity is calculated from the real permittivity (ε') and imaginary permittivity (ε'') by the formula [24]

$$\sigma_{ac} = \omega\varepsilon'\varepsilon_0 \tan\delta = \omega\varepsilon''\varepsilon_0 \tag{4}$$

where ω is the angular frequency and tan δ is the dielectric loss tangent. The increase in conductivity w.r.t. frequency is observed. This is a normal behaviour of the ferrites governed by the Jonscher law [25]. The increase in A.C. conductivity observed w.r.t. composition that indicates higher dielectric losses, hence higher absorption.

The impedance analysis of the ferrite with structural formula $BaFe_{12}O_{19}$ and $BaCo_{0.7}Ti_{0.7}Fe_{10.6}O_{19}$ is shown in Figs. 5 and 6, respectively. The input wave impedance (Z_i^*) calculations are based on the basis of the following equation [26]:

$$Z_i^* = Z_i' + jZ_i'' = Z_o\sqrt{\frac{\mu^*}{\varepsilon^*}}\tanh\left[j\frac{2\pi fd\sqrt{\mu^*\varepsilon^*}}{c}\right] \tag{5}$$

where Z_o is the characteristic impedance (377 Ω); μ^* and ε^* are the complex permeability and permittivity, respectively; f is the frequency in hertz; d is the thickness of the absorber layer; and c is the velocity of light in vacuum.

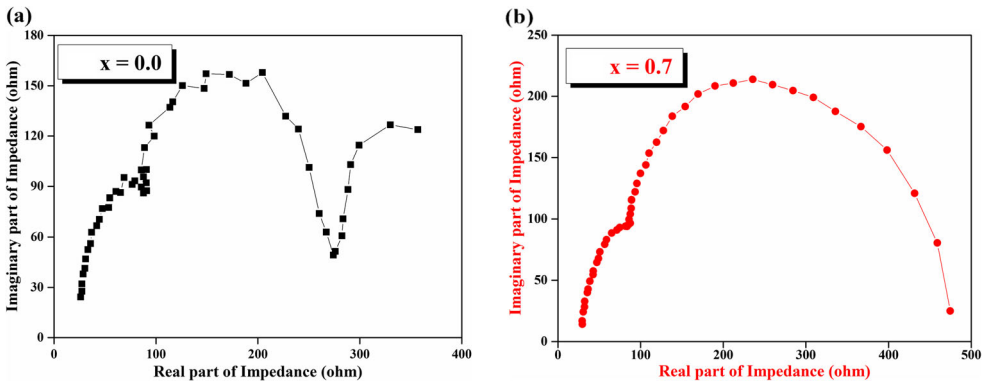

Fig. 5 Cole-Cole plot for impedance of ferrites with Co-Ti content: **a** $x = 0.0$ and **b** $x = 0.7$

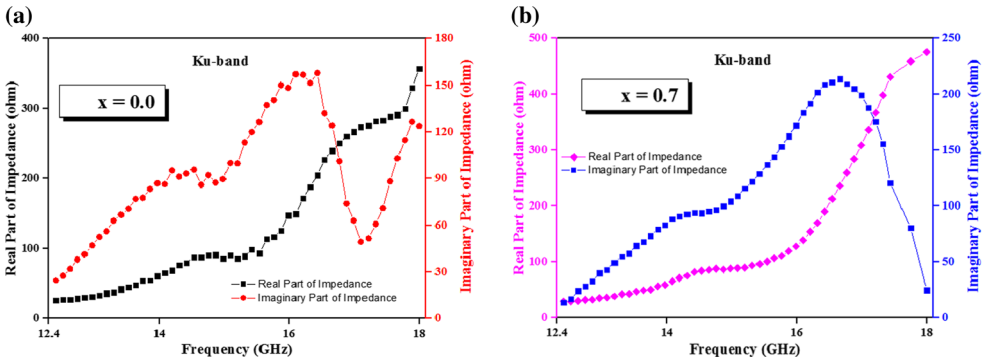

Fig. 6 Variation of real (Z') and imaginary (Z'') parts of impedance w.r.t. frequency for **a** $x = 0.0$ and **b** $x = 0.7$

Figure 5a shows two semi-circular arcs in $Z'' - -Z'$ plot for $x = 0.0$. This suggests that both grain bulk and grain boundaries contribute towards the conduction mechanism of ferrites. While Fig. 5b shows only one semi-circular arc for sample $x = 0.7$, that suggests the dominance of only grain boundaries in conduction process [27]. Since impedance plots of both the samples show perfect semi-circular arcs in Ku band, these ferrites exhibit a Debye type of relaxation [28]. Figure 6a, b shows the variation of real and imaginary parts of impedance w.r.t. frequency for these two samples. It is evident from the plots that real impedance continuously increases with an increase in frequency in Ku band, while imaginary impedance shows resonance peaks at 16.02 and 16.65 GHz frequency for samples $x = 0.0$ and $x = 0.7$, respectively. The increase in imaginary impedance suggests the increase in drain resistance with frequency [28]. It should be noted that absorption spectra of these two samples have observed maxima at the frequency where the real part of impedance is close to 377 Ω and the imaginary part is close to 0. The closer these two parameters to the specified values, the closer will be the system to the condition of impedance matching.

The frequency-dependent real permeability and imaginary permeability of the ferrites in 12.4–40 GHz range are depicted in Figs. 7 and 8, respectively. Absorption capability depends not only on the loss properties but also on the impedance matching performance. For impedance matching, complex permeability is as important parameter as complex permittivity [29]. The super-exchange interaction between ferric cations mediated by oxygen anions (Fe–O–Fe) gives rise to magnetism in the ferrites. The amplitude of this negative interaction depends on the angle between ferric cations and oxygen anions [30]. The lower values of permeability achieved in our analysis is due to a weak alternating field applied, resulting in weak super-exchange. With an increase in doping level, we have achieved enhancement

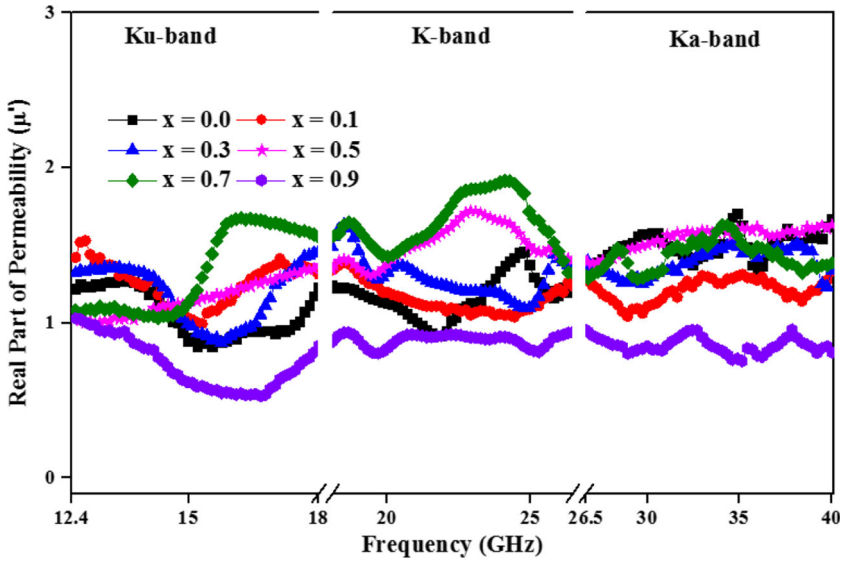

Fig. 7 Real permeability (μ') as a function of frequency and substitution for the synthesized ferrites

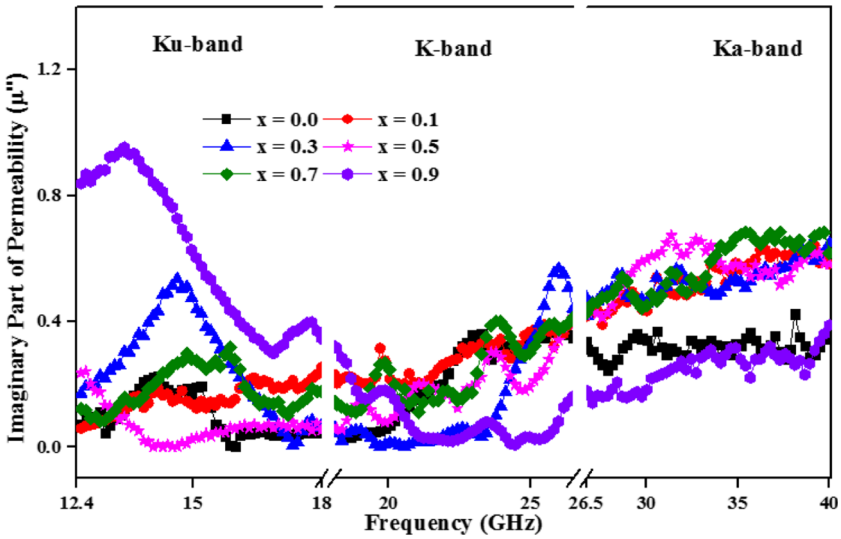

Fig. 8 Imaginary permeability (μ'') as a function of frequency and substitution for the synthesized ferrites

of real permeability, which is useful in realizing impedance match.

In ferrite materials, magnetic losses can originate due to various reasons like magnetic hysteresis, eddy current losses, domain wall displacement and magnetic resonances. Since a weak field is applied in the present case, the contribution of magnetic hysteresis is totally rejected. As these ferrites are multidomain as reported in the structural analysis of this series by Narang et al. [16], domain wall displacement could be the source of magnetism. Since barium hexaferrites are insulator, the eddy current contribution is not significant at all. The natural ferromagnetic resonance and exchange resonance are dominant at higher frequencies [31], and hence, these also can be responsible for the variation of imaginary permittivity in Ka band [32]. Pure barium hexaferrites have ferromagnetic resonance around 45 GHz. But, with doping, as the anisotropy constant has decreased (indicated from M–H loop analysis in [16]), ferromagnetic resonance frequency has also decreased. One noteworthy point in Figs. 2, 3, 4, 7 and 8 is that even with change in sample dimension, the plots are continuous at the frequency band boundaries. This is because permittivity and permeability are properties of material and are dimension-independent.

Reflection, transmission and absorption are a thickness-dependent parameter. So, the plots in Figs. 9, 10, 11, 12 and 13 are discontinuous on the band change (18 and 26.5 GHz). Figure 9 shows the frequency dependence of reflection loss

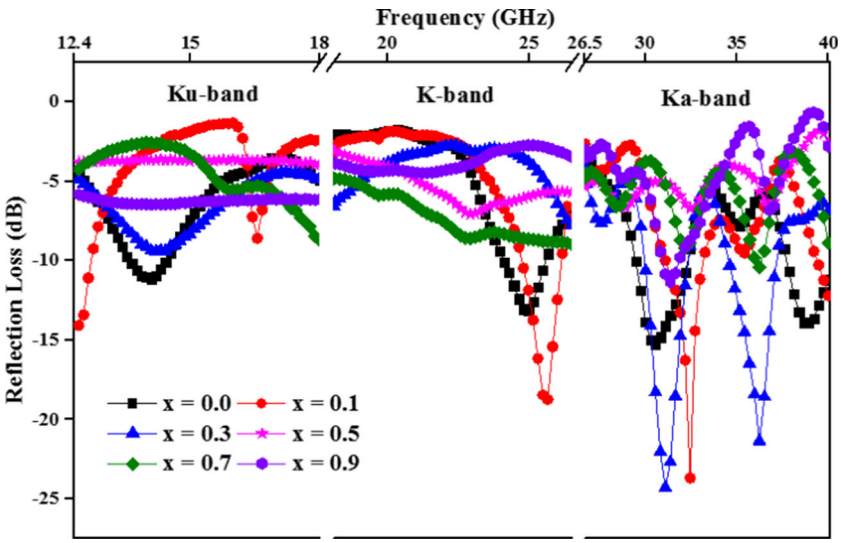

Fig. 9 Reflection loss (dB) observed in the ferrite pellets with different thicknesses for Ku (3.7 mm), K (3 mm) and Ka (2.5 mm) bands

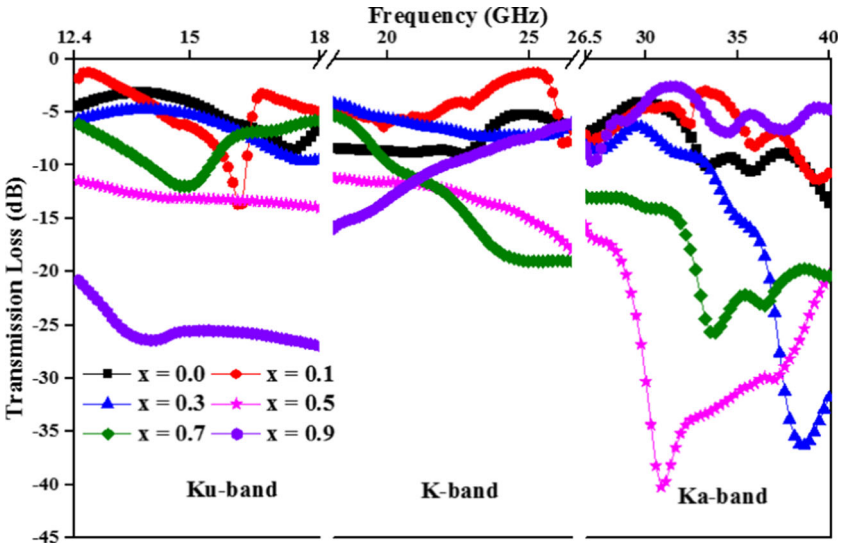

Fig. 10 Transmission loss (dB) observed in the prepared ferrites with different substitution levels of Co-Ti

(dB) observed in ferrite samples in the frequency region from 12.4 to 40 GHz. It can be seen from the plot that sample $x = 0.0$ has achieved a reflection loss of -11.13, -13.03 and -15.27 dB at 14.08, 24.08 and 30.55 GHz frequency, respectively. Sample $x = 0.1$ has achieved peaks of -14.07, -18.74 and -23.69 dB at 12.4, 25.65 and 32.44 GHz, respectively. A doped ferrite with $x = 0.3$ has owed a reflection loss of -24.28 and -21.34 dB at 31.09 and 36.22 GHz, respectively. One noteworthy thing here is that these results are experimentally determined, not the simulated one as done by most of the researchers [4, 6, 12, 19, 20]. The presented data is the experimental one. Reflection loss basically determines the ability of the material to reflect the EM energy. The lower the value of reflection loss, the lower will be the reflected power. Hence, the other ferrites, having a high value of reflection loss (>-10 dB), can be utilized in fabrication of reflecting surfaces at such high frequencies.

In this investigation of microwave absorption, we have adopted a waveguide measurement method without a back metal. So, only the reflection cannot determine the absorption capabilities of the material and the transmission loss has to be taken into account. So, in Fig. 10, we have presented the frequency dependence of transmission loss (dB) in Ku, K and Ka bands. The lower the transmission loss, the lower will be the power transmitted from the sample or received

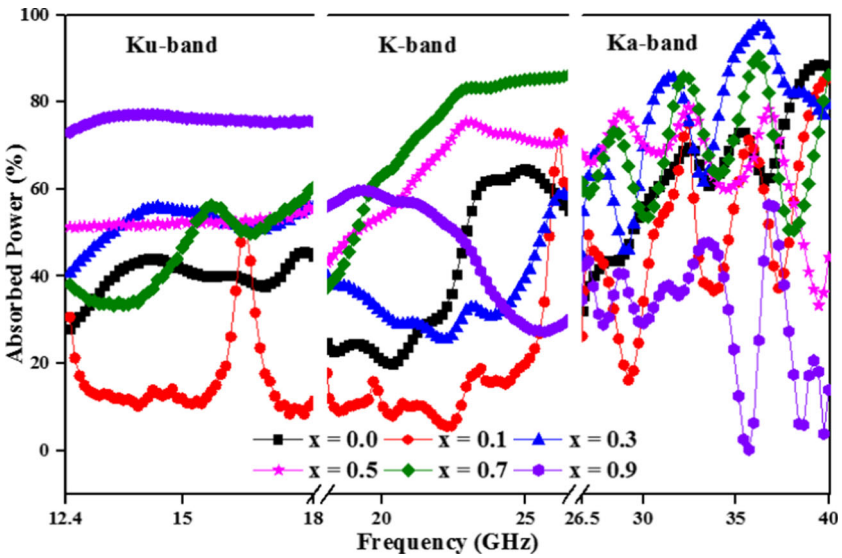

Fig. 11 Absorption ability of the prepared ferrites with different substitution levels of Co-Ti

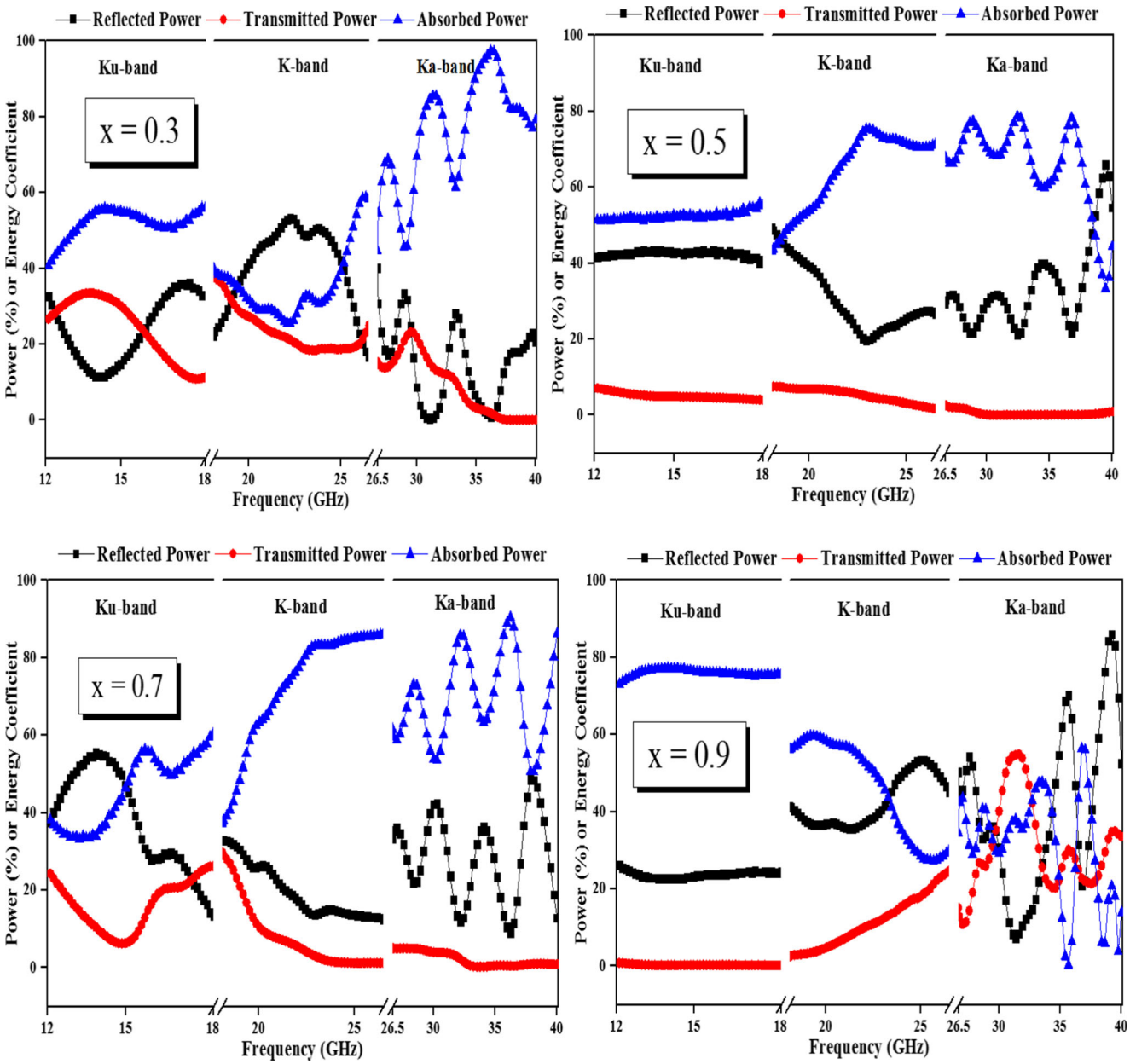

Fig. 12 Curves of power coefficients for samples with $x = 0.3$, 0.5, 0.7 and 0.9 in 12.4–40 GHz range

by the receiver. Samples $x = 0.5$ and 0.9 has the lowest values of transmission loss in Ku band. This shows that these samples do not allow the passage of EM energy from them in 12.4–18 GHz range. Samples $x = 0.3$, 0.5 and 0.7 also prevent the energy passage in Ka band. The sample with $x = 0.9$ has observed a low reflection loss in Ku band, so the combined power (reflected + transmitted power) is very small. This suggests the high absorption capability of this composition, as observed in Fig. 11. The experimental data (Fig. 12) in Ku band for sample $x = 0.9$ also agrees to this conclusion by showing high absorption. Similar analysis has been reported by Xu et al. [9].

Table 1 gives the values of maximum absorption peaks and reflection peaks for different ferrites with corresponding frequencies. It can be seen that the frequency of maximum absorption can be tuned with the substitution of cobalt and titanium ions. Thus, these ferrites can be implemented as frequency-tunable absorbers.

Figure 12 indicates the power division of incident power impinged on the surface of ferrite samples $x = 0.3, 0.5, 0.7$ and

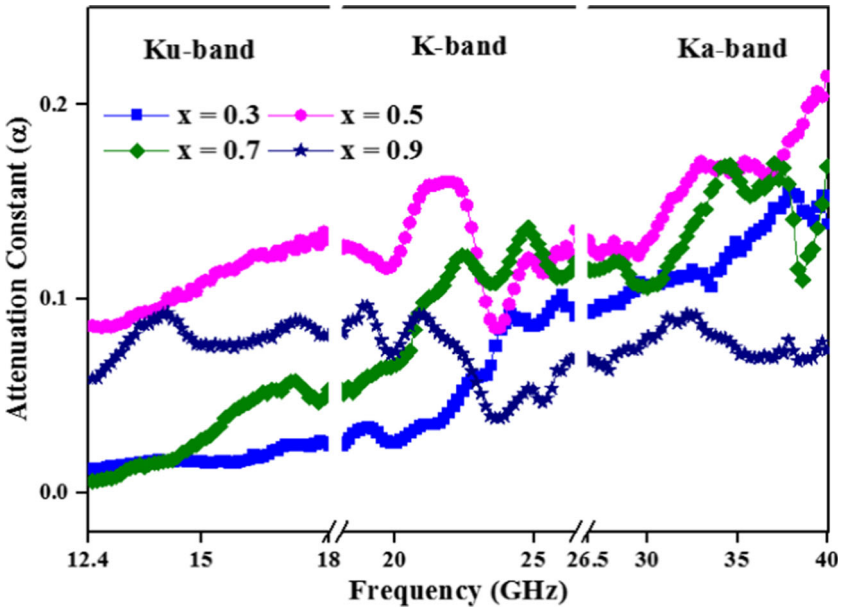

Fig. 13 Composition dependence of the attenuation constant (m^{-1}) of the Co-Ti-doped ferrites with $x =$ 0.3, 0.5, 07 and 0.9

0.9. This analysis helps to understand the usage of the prepared ferrite in specific application. If the reflected power is high in the sample, then it could be used in reflector application, and if the absorbed power is high, then it could be used in absorption applications. The average absorption (%) determined in sample $x = 0.3$ is 51.91, 35.08 and 75.74 % in Ku, K and Ka bands, respectively. Sample $x = 0.5$ absorbs 63.89 % of EM waves in K band and 65.66 % of waves in Ka band, respectively. Sample $x = 0.7$ has observed 45.74, 72.18 and 69.16 % absorption in these bands, respectively. A doped ferrite with $x = 0.9$ has shown the best absorption results (75.94 % average absorption) in Ku band. The calculations of these powers are based on the formula given in (1). A similar power analysis of the microwave absorber is reported by Folgueras [33]. Figure 12 indicates one major point that all the doped ferrites have very low transmission power in all the three bands. Thus, these ferrites prevent the passage of EM energy through it either by absorbing (most of the part) or reflecting (small part) it.

Attenuation constant (α) is calculated from the dielectric and magnetic properties of the materials in 12.4–40 GHz range using the formula [34]: $\alpha = (\sigma/2)\sqrt{|\mu^*|/|\varepsilon^*|}$. Figure 13 shows the variation of attenuation constant (in m^{-1}) of all the prepared ferrites with frequency. It can be seen in Fig. 13 that sample $x = 0.5$ has a higher value of α as compared to the other samples. This means that EM wave would reduce to a smaller extent faster as compared to the other samples. This conclusion is justified from Fig. 11 where this sample has a high value of absorption throughout the range. Also, sample $x = 0.9$ has also high attenuation constant in Ku band. The highest magnetic loss of this sample makes it the best absorber out of the prepared samples in Ku band.

Table 1 Average absorption (%) and reflection peaks of the different ferrite absorbers in 12.4–40 GHz range

Ferrite composition (x)	Maximum absorption peak (%)	Frequency of maximum absorption (GHz)	Best absorption result, % (frequency band)	Minimum reflection loss (dB)	Frequency of reflection peak (GHz)
$x = 0.0$	88.71	39.46	63.49 (Ka band)	−15.27	30.55
$x = 0.1$	85.58	40	51.23 (Ka band)	*−23.69*	32.44
$x = 0.3$	*97.37*	36.22	*75.74* (Ka band)	*−24.28*	31.09
$x = 0.5$	78.71	32.44	65.66 (Ka band)	−7.06	22.93
$x = 0.7$	*90.45*	36.22	*72.18* (K band)	−10.43	36.22
$x = 0.9$	77.29	14.08	*75.94* (Ku band)	−11.43	31.36

4 Conclusion

Co-Ti-substituted barium hexaferrites have been analysed using a rectangular waveguide measurement technique in 12.4–40 GHz frequency range. The analysis of complex permittivity variation has shown that substitution of impurity atoms has improved the dielectric losses and reduced the dielectric constant in the material. Imaginary permeability has increased with doping that can be attributed to the domain wall displacement and ferromagnetic resonances. Impedance analysis suggests the dominance of grain boundaries in all the ferrites, while grain contribution is significant only in an undoped ferrite. Samples $x = 0.1$ and $x = 0.3$ owe reflection peaks of -23.69 and -24.28 dB at 32.44 and 31.09 GHz, respectively. Samples $x = 0.3$, 0.7 and 0.9 show an average absorption of 75.74, 72.18 and 75.94 % in Ka, K and Ku bands, respectively. Absorption peaks as high as 97.37 and 90.45 % are observed in samples $x = 0.3$ and $x = 0.7$, respectively. All these points lead us to a conclusion that these materials can be used as a single-layer frequency-tunable absorber in military, wireless communication and radar stealth technology.

References

1. Ni, S., Sun, X., Wang, X., Zhou, G., Yang, F., Wang, J., He, D.: Mater. Chem. Phys. **124**, 353–358 (2010)
2. Narang, S.B., Hudiara, I.S.: J. Ceram. Process. Res. **7**(2), 113–116 (2006)
3. Emerson, W.L.: IEEE Trans. Antennas Propag. **21**(4), 484–490 (1973)
4. Alam, R.S., Moradi, M., Rostami, M., Nikmanesh, H., Moayedi, R., Bai, Y.: J. Magn. Magn. Mater. **381**, 1 (2015)
5. Peng, C.H., Hwang, C.C., Wan, J., Tsai, J.S., Chen, S.Y.: J. Mater. Sci. Engg. B **117**(1), 27–36 (2005)
6. Folgueras, L.C., Alves, M.A., Rezende, M.C.: J. Aerosp. Technol. Manag. **2**(1), 63–70 (2010)
7. Balanis, C.A.: Advanced engineering electromagnetics. John Wiley Sons, New York (1989)
8. Hippel, A.: Von Hipple Dielectric materials and applications. London, Artech House (1954)
9. Xu, F., Bai, Y., Jiang, K., Qiao, L.: Int. J. Miner. Metall. Mater. **19**(5), 453–456 (2012)
10. Kovetz, A.: Electromagnetic theory. New York Oxford (2000)
11. Narang, S.B., Chawla, S.K., Mudsainiyan, R.K., Pubby, K.: Integr. Ferroelectr **167**(1), 98–106 (2015)
12. Kiani, E., Rozatian, A.S.H., Yousefi, M.H.: J. Magn. Magn. Mater. **361**, 25–29 (2014)
13. Singh, C., Narang, S.B., Hudiara, I.S., Sudheendran, K., Raju, K.C.J.: J. Magn. Magn. Mater. **320**(10), 1657–1665 (2008)
14. Jamalian, M., Ghasemi, A., Paimozd, E.: Curr. Appl. Phys. **14**, 909–915 (2014)
15. Singh, C., Narang, S.B., Hudiara, I.S., Sudheendran, K., Raju, K.C.J.: J. Electroceram. **27**(3-4), 120–125 (2011)
16. Narang, S.B., Kaur, P., Bahel, S., Singh, C.: J. Magn. Magn. Mater. **405**, 17 (2016)
17. Lee, Y.S., Malek, F., Cheng, E.M., Liu, W.W., You, K.Y., Iqbal, M.N., Wee, F.H., Khor, S.F., Zahid, L., Malek, M.F.B.H.A.: Progress Electromagn. Res. **140**, 795–812 (2013)
18. Nicolson, A.M., Ross, G.F.: IEEE Trans. Instrum. Meas. **19**, 377–382 (1970)
19. Ahmed, M., Grössinger, R., Kriegisch, M., Kubel, F., Rana, M.U.: J. Magn. Magn. Mater. **332**, 137–145 (2013)
20. Guo, F., Ji, G., Xu, J., Zou, H., Gan, S., Xu, X.: J. Magn. Magn. Mater. **324**, 1209–1213 (2012)
21. Dong, C., Wang, X., Zhou, P., Liu, T., Xie, J., Deng, L., Magn, J.: Magn. Mater. **354**, 340–344 (2014)
22. Devan, R.S., Ma, Y.R., Chougule, B.K.: Mater. Chem. Phys. **115**(1), 263–268 (2009)
23. Tang, X., Zhao, B.Y., Tian, Q., Hu, K.A.: J. Phys. Chem. Solid **67**(12), 2442–2447 (2006)
24. Yusoff, A.N., Abdullah, M.H., Ahmad, S.H., Jusoh, S.F., Mansor, A.A., Hamid, S.A.A.: J. Appl. Phys. **92**(2), 876–882 (2002)
25. Jonscher, A.K.: Universal relaxation law. Chelsea Dielectric, London (1996)
26. Yang, X.F., Jin, Q., Chen, Z.P., Li, Q.L., Liu, B.: J. Magn. Magn. Mater. **367**, 64–68 (2014)
27. Narang, S.B., Kaur, D., Pubby, K.: Ferroelectrics **486**(1), 74–85 (2015)
28. Saha, S., Chanda, S., Dutta, A., Sinha, T.P.: Mater. Res. Bull. **48**(11), 4917–4923 (2013)
29. Vinayasree, S., Soloman, M.A., Sunny, V., Mohanan, P., Kurian, P., Joy, P.A., Anantharaman, M.R.: J. Appl. Phys. **116**, 024902 (2014)
30. Harris, V.G., Chen, Z., Chen, Y., Yoon, S., Sakai, T., Gieler, A., Yang, A., He, Y.: J. Appl. Phys. **99**, 08M911 (2006)
31. Sadiq, I., Ali, I., Rebrov, E., Naseem, S., Ashiq, M.N., Rana, M.U.: J. Magn. Magn. Mater. **370**, 25–31 (2014)
32. Duan, M.C., Yu, L.M., Sheng, L.M., An, K., Ren, W., Zhao, X.L.: J. Appl. Phys. **115**, 174101 (2014)
33. Folgueras, L.C., Alves, M.A., Rezende, M.C.: Mater. Res. **13**(2), 197–201 (2010)
34. Jordan, E.C., Balmain, K.G.: Electromagnetic waves and radiating systems. Prentice Hall, New Delhi (2003)